

Alma Mater Studiorum Università di Bologna  
Archivio istituzionale della ricerca

In-field and non-destructive monitoring of grapes maturity by hyperspectral imaging

This is the final peer-reviewed author's accepted manuscript (postprint) of the following publication:

*Published Version:*

Benelli A., Cevoli C., Ragni L., Fabbri A. (2021). In-field and non-destructive monitoring of grapes maturity by hyperspectral imaging. BIOSYSTEMS ENGINEERING, 207(July 2021), 59-67 [10.1016/j.biosystemseng.2021.04.006].

*Availability:*

This version is available at: <https://hdl.handle.net/11585/831926> since: 2024-04-09

*Published:*

DOI: <http://doi.org/10.1016/j.biosystemseng.2021.04.006>

*Terms of use:*

Some rights reserved. The terms and conditions for the reuse of this version of the manuscript are specified in the publishing policy. For all terms of use and more information see the publisher's website.

This item was downloaded from IRIS Università di Bologna (<https://cris.unibo.it/>).  
When citing, please refer to the published version.

(Article begins on next page)

# In-field and non-destructive monitoring of grapes maturity by hyperspectral imaging

Alessandro Benelli<sup>a</sup>, Chiara Cevoli<sup>a,b\*</sup>, Luigi Ragni<sup>a,b</sup>, Angelo Fabbri<sup>a,b</sup>

<sup>a</sup>*Department of Agricultural and Food Sciences, Alma Mater Studiorum, University of Bologna, Piazza Goidanich 60, Cesena, 47521, Italy*

<sup>b</sup>*Interdepartmental Centre for Agri-Food Industrial Research, Alma Mater Studiorum, University of Bologna, Via Quinto Bucci 336, Cesena, 47521, Italy*

\*Corresponding author: chiara.cevoli3@unibo.it

## Abstract

Monitoring the quality attributes of grapes is a practice that allows the state of ripeness to be checked and the optimal harvest time to be identified. A non-destructive method based on hyperspectral imaging (HSI) technology was developed. Analyses were carried out directly in the field on a ‘Sangiovese’ (*Vitis vinifera* L.) vineyard destined for wine production, by using a Vis/NIR (400–1000 nm) hyperspectral camera. One vineyard row was analysed on 13 different days during the pre-harvest and harvest time. The soluble solids content (SSC) expressed in terms of °Brix was measured by a portable digital refractometer. Afterwards, the grape samples were split in two classes: the first one composed by the samples characterised by a °Brix lower than 20 (not-ripe), while the second one by the samples with a °Brix higher than 20 (ripe). Grape mean spectra were extracted from each hyperspectral image and used to predict the SSC by partial least squares regression (PLS), and to classify the samples into the two classes by PLS discriminant analysis (PLS-DA). SSC was predicted with a  $R^2=0.77$  (RMSECV=0.79 °Brix), and the samples were correctly classified with a percentage from 86 to 91%. Even if the number of wavelengths was limited, the percentages of correctly classified samples were again within the above-mentioned range. The present study shows the

potential of the use of HSI technology directly in the field by proximal measurements under natural light conditions for the prediction of the harvest time of the ‘Sangiovese’ red grape.

**Keywords:** hyperspectral, in-field, grape, wine, harvest, classification

## **1. Introduction**

Italy is the largest wine producer in the world, with a production in 2018 of 5,480 million litres (18.8% of world production) (OIV International Organisation of Vine and Wine, 2019). In an industrialised wine growing system, monitoring the quality attributes, such as soluble solids content (SSC), acidity and anthocyanin content of grapes is extremely important: well-planned monitoring allows to check the growth and ripening of the grapes, and finally to decide when to proceed with the harvest (Delrot, Medrano, Or, Bavaresco, Grando, 2010). For instance, by managing irrigation through the use of techniques such as the regulated deficit irrigation, significant increases in SSC and anthocyanins can be achieved which together with a decrease in yield and berry size can lead to substantial improvements in grape quality (Acevedo-Opazo, Ortega-Farias, Fuentes, 2010; Pellegrino, Lebon, Simonneau, Wery, 2005).

Monitoring of grape quality attributes can be carried out directly in the field using traditional destructive techniques. Alternatively, quality attributes can be estimated by non-destructive techniques, such as near-infrared (NIR) spectroscopy. Portable NIR instruments were used to determine the following quality attributes of grapes: water content, SSC, reductant sugars, pH, titratable acidity, maturity index (sugar/acidity ratio), extractable anthocyanins, potential anthocyanins (Teixeira Dos Santos, Lopo, Páscoa, Lopes, 2013).

Over the last two decades the use of HSI technology in the quality assessment of fruits and vegetables has become of increasing interest (Chandrasekaran, Panigrahi, Ravikanth, Singh, 2019; Liu, Zeng, Sun, 2015). HSI was initially limited to controlled environments such as laboratories but gradually,

53 thanks to the miniaturisation and improved computing and data storage capabilities, it began to be  
54 used directly in the field (Benelli, Cevoli, Fabbri, 2020). Hyperspectral images can be captured either  
55 remotely by airborne vehicles and unmanned aerial vehicles (Ishida et al., 2018; Matese & Di  
56 Gennaro, 2015; Zarco-Tejada et al., 2013) or by ground vehicles (Deery, Jimenez-Berni, Jones,  
57 Sirault, Furbank, 2014; Gutiérrez, Fernández-Novales, Diago, Tardaguila, 2018a; Huang, Lee,  
58 Thomson, Reddy, 2016; Jay et al., 2017; Underwood, Wendel, Schofield, McMurray, Kimber, 2017;  
59 Wendel, Underwood, Walsh, 2018; Whetton, Waine, Mouazen, 2018), which produces proximal  
60 hyperspectral images with high spatial resolution. Proximal HSI could therefore allow non-  
61 destructive, contactless, and automated monitoring of grape quality attributes. Moreover, the  
62 acquisition of hyperspectral images can be performed continuously, enabling the rapid scanning of  
63 large areas. Hyperspectral data is characterised by two spatial and one spectral dimension, therefore  
64 only specific regions of interest (ROIs) can be selected, and the residual regions can be excluded. In  
65 this sense, hyperspectral analysis is useful to guide the choice of true multispectral less expensive  
66 solutions.

67 Concerning in-field grape studies, Gutiérrez et al. (2018a) adopted an on-the-go HSI system for the  
68 classification of 30 grapevine varieties directly acquired in the field. Through the development of  
69 classification models based on support vector machines (SVM) and multilayer perceptron (MLP),  
70 prediction performance (F1 score) up to 0.99 was achieved. The same on-the-go HSI system  
71 described above, combined with SVM, was adopted to estimate SSC and anthocyanin concentration  
72 of wine grapes (Gutiérrez et al., 2018b). Determination coefficients ( $R^2$ ) of 0.92 (RMSE=1.274 °Brix)  
73 and 0.83 (RMSE=0.211 mg g<sup>-1</sup>) were obtained for the prediction of SSC and anthocyanin  
74 concentration, respectively. These two studies highlight the potential of HSI to monitor the indices  
75 of grape ripening directly in the field and therefore to improve vineyard decisions and management.  
76 Non-linear statistical methods were used in both studies. Considering the results just mentioned, it  
77 would be interesting to investigate whether, even combining HSI with linear methods and reducing  
78 the number of wavelengths, it is possible to monitor the degree of grape maturity directly in the field.

Furthermore, considering a possible application of this technique, a simple binary model able to simply determine whether grapes are ripe for harvesting could be interesting.

Thus, the present study aims to identify the proper degree of ripeness, suitable for harvesting wine grapes, through the observation of the SSC evolution by means of HSI technology applied directly in the field. The mean spectra were extracted from each hyperspectral image and used to predict the SSC and to classify the samples into the two classes (not-ripe and ripe), by partial least squares regression (PLS) and discriminant analysis (PLS-DA), respectively.

## **2. Materials and methods**

### *2.1 Samples*

One side of a row of ‘Sangiovese’ (*Vitis vinifera* L.) grape vineyards, located near Cesena, Italy, was analysed on 13 different days in the period between August 20<sup>th</sup> and October 4<sup>th</sup>, 2019 (from pre-harvest to harvest time). The row was divided into 11 sections; from each section 3, grapes were taken for each day of analysis, for a total of 429 samples.

### *2.2 Hyperspectral acquisitions*

The adopted push-broom hyperspectral camera (Nano-Hyperspec VNIR, Headwall Photonics, Inc., Fitchburg, MA, USA) scans single lines in a sequence, each one consisting of 640 voxels: the image is created by moving the camera along the scanning direction (Fig. 1a). Each voxel contains, in addition to the two spatial dimensions, a Vis/NIR spectrum (400–1000 nm) characterized by 272 spectral bands, with a nominal spectral resolution of 2.2 nm. The mounted lens has an effective focal length of 17 mm, with the optical axis perpendicular to the side of the vineyard row (scanned surface) analysed (Figure 1b). The camera was installed on a garden cart (Fig. 1b) 120 cm above the ground and it was powered by a 12 V, 45 Ah automotive battery through a DC to AC power inverter. The scans were performed at about 1.6 m from the side of the vineyard row.

104 Direct sunlight with clear sky conditions, was used as a light source. To reduce the fluctuation of the  
105 sample temperature, all the acquisitions were carried during the same period of the day, from  
106 10:30 a.m. to 12:00 p.m.

107 The frame rate was set to approximately 100 frames s<sup>-1</sup>. The exposure time was set from 6 to 8 ms,  
108 depending on the light intensity, and was achieved through calibration, by framing a white high-  
109 reflectance matter panel, placed at the same distance as the vineyard row, to cover the entire angle of  
110 view of the camera. Given the clear sky conditions and the short time required, about 10 min,  
111 acquisition of hyperspectral images of the 11 vineyard row sections and calibration was carried out  
112 only once per day.

113 The raw diffuse reflectance spectrum ( $R_R$ ) was extracted from the HS images. The calibrated diffuse  
114 reflection spectrum ( $R_C$ ) was calculated by applying the following equation:(Guo et al., 2019):

$$115 \quad R_C = \frac{R_R - R_D}{R_W - R_D} \quad (1)$$

116 where  $R_D$  is the reflectance spectrum of dark reference, obtained by applying the cap on the lens;  $R_W$   
117 is the reflectance spectrum of white reference, obtained by means calibration with the white high-  
118 reflectance matte panel reported above.

119 A hyperspectral image from each of the 11 sections obtained from the vineyard row, was acquired  
120 per day of analysis (Fig. 1c): therefore, during the 13 d of analysis, a total of 143 vineyard row sections  
121 were scanned.

122

### 123 *2.3 Soluble solids content measurement*

124 After the acquisition of the images, the SSC, expressed in °Brix, was measured on 3 grape berries  
125 (randomly selected) from each of the 11 sections by using a portable digital refractometer (PR-101  
126 Digital Refractometer, ATAGO CO., LTD, Tokyo, Japan). Subsequently, the mean for each section  
127 was calculated.

128 One-way analysis of variance (ANOVA) with Tukey-HSD post-hoc test (p-level < 0.05) was applied  
129 to evaluate significant differences between SSC means over the different days of analysis.

## 2.4 Hyperspectral images elaboration

ROI selection was made using the software HyperCube, v. 11.52 (U.S. Army Engineer Research and Development Center (ERDC), USA). For each image, 5 points and a maximum of a further 120 adjacent points (11 x 11 voxels matrix, with the selected point in the centre of the matrix) were selected on 5 different berries directly illuminated by the sun, not in the shade. The (reference) points included in the classification were characterized by a metric distance from the mean (signature) spectrum of the manually selected points within the range (tolerance threshold) [0,0.04] (Fig. 2). The metric distance was calculated by applying the absolute difference (Manhattan) function (Eq. (2)) (Deborah, Richard, Hardeberg, 2015) and normalised in the range [0,1].

$$d(R_1, R_2) = \sum_{\lambda} |R_{1,\lambda} - R| \quad (2)$$

where  $R_1, R_2$  are two reflectance spectra.

From the spectra of the classified points, the mean spectrum for each hyperspectral image was calculated.

The spectral bands between 400–424 nm were omitted as a result of the low signal-to-noise ratio produced by the sensor, as reported in Wendel et al. (2018). The spectra were smoothed (Savitzky-Golay method; polynomial order: 2; smoothing points: 15) to reduce noise from the spectra and following pre-treated by the standard normal variate (SNV) method, first derivative (D1) and finally mean centred (MC). The SNV is one of the most common pre-processing method used to correct spectra for changes in optical path length and light scattering, while the derivatives have the capability to remove both additive and multiplicative effects in the spectra (Rinnan, van den Berg, Engelsen, 2009). After SNV, each spectrum will have a mean of 0 and a standard deviation of 1.

Principal component analysis (PCA) was applied to the mean spectra as exploratory technique to visualize the data according to °Brix and time evolution. Subsequently, a preliminary PLS regression model was built to estimate the SSC. The validation was carried out by the venetian blind cross-validation method (segments: 10).

155 PLS-DA models were built to classify the samples according to °Brix. In particular, classification  
156 models with 2 categories (not-ripe and ripe) were developed: according to Bucelli, Costantini and  
157 Storchi (2010), the first class was composed by the samples characterized by a °Brix lower than 20  
158 (0), while the second one by the samples with a °Brix equal or higher than 20 (1).  
159 The sample dataset (n = 143) was split in calibration (venetian blinds cross-validation, including 75%  
160 of the samples) and external validation set (25% of the samples) by using the Onion method  
161 (Gallagher et al., 2004). The threshold value, able to identify the belonging category of each sample  
162 into one of the groups, was defined by using a probabilistic approach based on Bayes's rule. To avoid  
163 the model over-fitting, the optimal number of latent variables were chosen by plotting the root mean  
164 square error of cross-validation (RMSECV) as a function of the number of components and by  
165 identifying where the curve reaches a local minimum. The receiver operating characteristic (ROC)  
166 curves in prediction were evaluated to assess the goodness of the models.  
167 All the chemometrics models were developed by using PLS Toolbox for Matlab2018a.

168

### 169 **3. Results and discussion**

170 Means and standard deviation of the °Brix measured during the 13 d of analysis are reported in Table  
171 1. The increase between the first and last day was of 27.5%, from 17.8 °Brix (day I) to 22.7 °Brix  
172 (day XIII). Several significant differences between the °Brix mean values were achieved over the  
173 different days of analysis. The whole data set was characterized by a mean value of  $20.6 \pm 1.7$  °Brix,  
174 which make suitable to split it in two subsets with a threshold of 20 °Brix.

175 Raw and pre-treated (smoothing and SNV) mean spectra of all the samples by day of analysis are  
176 presented in Fig. 3. In the Vis/NIR region (400–1000 nm), the visible spectrum (400–700 nm)  
177 presents the absorption bands of some substances used as ripening indexes of fruit: anthocyanins at  
178 around 500 nm, carotenoids at 570–590 nm, and chlorophyll *a* at 680–710 nm (ElMasry, Wang,  
179 ElSayed, Ngadi, 2007; Munera et al., 2017). In the NIR region (700–1000 nm), absorption bands of  
180 water at 760 nm and 960–970 nm are characterised by the overtone of O-H bonds (McGlone &



181 Kawano, 1998; Nicolaï et al., 2007): since the water content of a ripe wine grape is 70–80% (FAO  
182 Food and Agriculture Organization, 2009), it can be expected that the water related absorption band  
183 will prevail. Absorption band around 840 nm was associated with sugar (Pu, Liu, Wang, Sun, 2016);  
184 moreover, peaks observed in the 950–1000 nm region were related to both water and carbohydrates,  
185 as the second overtone of O-H and N-H, a combination band of O-H bonds and the third overtone of  
186 C-H, were found in the region (Camps & Christen, 2009). As observed, the water absorption peaks  
187 in the NIR (700–1000 nm) spectral region are not very marked and wide. Therefore, spectral  
188 information from SSC in the 800–1000 nm range will tend to be less covered by water (Camps &  
189 Christen, 2009; Manley, Joubert, Myburgh, Kidd, 2007).

190 The score plot of the first two principal components (PC1: 59%; PC2: 28%) resulting from PCA  
191 shows the samples distribution according to the day of analysis. A tendency to place the samples from  
192 left to right can be observed on PC1, starting from day I (quadrant III) to day XIII (quadrant IV)  
193 (Figure 4a).

194 A similar distribution can be observed according to the SSC: the samples are distributed along PC1,  
195 mainly on the left those with  $\text{SSC} < 20^\circ\text{Brix}$  (quadrants II and III), on the right those with  
196  $\text{SSC} \geq 22^\circ\text{Brix}$  (quadrants I and IV) (Fig. 4b).

197 The best PLS results were obtained pre-treating the spectra by SNV + MC. Particularly,  $R^2 = 0.768$   
198 and  $\text{RMSECV} = 0.79^\circ\text{Brix}$  were achieved in cross-validation with 7 latent variables. Figure 5 shows  
199 the predicted versus measured  $^\circ\text{Brix}$  values.

200 These results agree with those present in literature and developed by using spectra in the same  
201 wavelength range and acquired directly in-field. Furthermore, regardless of the  $R^2$  values, the RMSE  
202 is substantially lower. Diezma-Iglesias, Barreiro, Blanco and García-Ramos (2008) predicted SSC on  
203 480 samples of ‘Cabernet Sauvignon’ by using a portable hand-held spectrometer (590–1090 nm),  
204 reporting a  $R^2 = 0.72$ , while Guidetti, Beghi and Bodria (2010) working with a simple Vis/NIR system  
205 in the range from 400 to 1000 nm, obtained in prediction  $r=0.82$  ( $R^2=0.67$ ) and  $\text{RMSEP}=1.48^\circ\text{Brix}$ .  
206 Gutiérrez et al. (2018b) used the HSI technique (400–1000 nm) to measure SSC in wine grapes in

207 real time.  $R^2$  of 0.91 (RMSE = 1.358 °Brix) and 0.92 (RMSE = 1.274 °Brix) were achieved in cross  
208 validation and prediction, respectively, by using the SVM techniques.

209 PLS-DA results, in terms of percentage of correctly classified samples, are reported in Table 2. The  
210 percentages ranged from 86 to 91%. Considering the prediction set, the best result was obtained  
211 applying as pre-treatment the SNV + MC. The results obtained with the hyperspectral technique  
212 improved those achieved by Guidetti et al. (2010) by using of a portable contact system. The authors  
213 combined Vis/NIR spectroscopy in the wavelength range 450 – 980 nm with PLS-DA to classify  
214 grape samples in two groups based on SSC (threshold = 21 °Brix), obtaining a percentage of samples  
215 correctly classified (in prediction) of 77.1% (Guidetti et al., 2010).

216 The ROC curves in prediction (Fig. 6) summarise the trade-off between specificity (number of  
217 samples predicted to not be in the class divided by the actual number not in the class) and sensitivity  
218 (number of samples predicted to be in the class divided by number actually in the class) for the PLS-  
219 DA classification models. The area under the curves (AUC = 0.9855 for SNV + MC and  
220 AUC = 0.9578 for SNV + D1 + MC) suggest that the models were characterised by a high degree of  
221 discrimination, confirming that the best model was those developed considering only the SNV + MC  
222 as pre-treatment.

223 Results, in terms of probability (Bayes's rule) of belonging to the class °Brix < 20, are shown in Fig.  
224 7. The higher a sample is placed, the higher the probability that it will be classified as a member of  
225 the °Brix < 20 class. Consequently, samples classified as members of the other class (°Brix  $\geq$  20)  
226 are placed at the bottom of the graph. The threshold value (dotted red line) was set at 0.5 (probability  
227 of 50%); samples with a probability lower than this value are considered improperly classified.

228 Considering the SNV + MC and SNV + D1 + MC pre-treatments, 89% and 77% of the samples (in  
229 prediction) were classified with a probability higher than 70%.

230 Figure 8 shows the VIP (variable importance in projection) scores obtained by the PLS-DA models.  
231 These scores estimate the importance of each variable in the projection used in the PLS-DA model.  
232 A variable with a VIP score close to or higher than 1 can be considered important in a given model.

For both the pre-treatments, similar regions with VIP score higher than 1 were obtained, suggesting that the wavelengths with the highest contribution are in the NIR region of the spectrum (from 700 to 1000 nm). Consequently, the variable selection method based on the VIP scores higher than 1 was used to reduce the original data set.

PLS-DA results (percentage of correctly classified samples) obtained by using the reduced number of variables (wavelengths), are reported in Table 3. In particular, 93 (SNV + MC) and 88 (SNV + D1 + MC) x-variables were used to develop the new PLS-DA. The percentages of correctly classified samples are slightly lower (from 86 to 91%) than those obtained considering the whole spectrum. However, the results are still completely acceptable. This confirms also by the high AUC values (0.939 and 0.942).

This work presents a solution for in-field and non-destructively determination of grape maturity degree by using HSI combined with linear chemometric techniques. Particularly, the results confirm the suitability for estimating the soluble solid content of red grapes.

The positioning of the vineyard row did not create any obstacles regarding the direct solar lighting of the grape bunches. The images along the vineyard row were acquired in the NNE-SSO direction, with the row on the right-hand side of the scanning direction. Consequently, the suitable period for analysis was during the late morning and not later than midday. To scan the other side of the row, it would have been necessary to proceed after midday. Shadows also did not present any problems, as the sun was behind the camera at the time of the acquisitions. To correctly acquire hyperspectral images, the vines should be stripped to ensure that the upper leaves do not overshadow the grapes below. Grapes often had reflection and shaded areas, which need to be excluded during the selection of the ROIs, along with fully or partially shaded grape bunches. In the presence of clouds or even just a slight cloud cover, a significant variation in light intensity was observed: this means that the camera would need to be recalibrated every time a section of the row was scanned. In addition, it is possible that the brightness conditions change soon after calibration, so it would be necessary to recalibrate and immediately proceed with the scan of the row section.

259 The variability grape of a vineyards, in terms of SCC, often is quite high. This depends on many  
260 factors, such us the vineyards orientation, unevenness of the land and meteorological phenomena. For  
261 this reason, the grapes are harvested at different times even along the same row. Consequently, to  
262 optimise the harvest, a technique that allows to have a mapping of the SCC for all grapes, would  
263 certainly be an advantage.

264

#### 265 **4. Conclusions**

266 Hyperspectral imaging technology, usually adopted in laboratories with auxiliary artificial lighting,  
267 was used in-field under natural lighting conditions to monitor the maturity degree of ‘Sangiovese’  
268 (*Vitis vinifera* L.) grapes. The results achieved confirm that it is possible to predict the soluble solid  
269 content and to classify grape samples into two classes (not-ripe and ripe) using a linear technique to  
270 elaborate the spectral data. Furthermore, the classification performance remained substantially  
271 unchanged by reducing the number of wavelengths, so it is expected that a less expensive  
272 multispectral camera in the 400–1000 nm range can work just as well. The implementation of a  
273 hyperspectral imaging system on an agricultural vehicle coupled to a gimbal stabilisation system,  
274 together with the development of hyperspectral image segmentation techniques, would allow  
275 on-the-go analysis of large vineyard extensions. Attention should be paid to the presence of water on  
276 the surface of the sample under analysis, to the presence of variable cloudiness and, if the leaves are  
277 analysed, to the presence of wind.

278

279 **Declarations of interest: none.**

280

#### 281 **References**

282 Acevedo-Opazo, C., Ortega-Farias, S., & Fuentes, S. (2010). Effects of grapevine (*Vitis vinifera* L.)  
283 water status on water consumption, vegetative growth and grape quality: An irrigation scheduling

284 application to achieve regulated deficit irrigation. *Agricultural Water Management*, 97(7), 956–964.  
285 <https://doi.org/10.1016/j.agwat.2010.01.025>  
286

287 Benelli, A., Cevoli, C., & Fabbri, A. (2020). In-field hyperspectral imaging: An overview on the  
288 ground-based applications in agriculture. *Journal of Agricultural Engineering*, LI(1030), 129–139.  
289 <https://doi.org/10.4081/jae.2020.1030>  
290

291 Bucelli, P., Costantini, E. A. C., & Storchi, P. (2010). It is possible to predict sangiovese wine quality  
292 through a limited number of variables measured on the vines. *Journal International Des Sciences de*  
293 *La Vigne et Du Vin*, 44(4), 207–218. <https://doi.org/10.20870/oeno-one.2010.44.4.1473>  
294

295 Camps, C., & Christen, D. (2009). On-tree follow-up of apricot fruit development using a hand-held  
296 NIR instrument. *Journal of Food, Agriculture and Environment*, 7(2), 394–400.  
297

298 Chandrasekaran, I., Panigrahi, S. S., Ravikanth, L., & Singh, C. B. (2019). Potential of Near-Infrared  
299 (NIR) Spectroscopy and Hyperspectral Imaging for Quality and Safety Assessment of Fruits: an  
300 Overview. *Food Analytical Methods*, 12(11), 2438–2458. [https://doi.org/10.1007/s12161-019-](https://doi.org/10.1007/s12161-019-01609-1)  
301 [01609-1](https://doi.org/10.1007/s12161-019-01609-1)  
302

303 Deborah, H., Richard, N., & Hardeberg, J. Y. (2015). A Comprehensive Evaluation of Spectral  
304 Distance Functions and Metrics for Hyperspectral Image Processing. *IEEE Journal of Selected Topics*  
305 *in Applied Earth Observations and Remote Sensing*, 8(6), 3224–3234.  
306 <https://doi.org/10.1109/JSTARS.2015.2403257>  
307

308 Deery, D., Jimenez-Berni, J., Jones, H., Sirault, X., & Furbank, R. (2014). Proximal remote sensing  
 309 buggies and potential applications for field-based phenotyping. *Agronomy*, 4(3), 349–379.  
 310 <https://doi.org/10.3390/agronomy4030349>  
 311

312 Delrot, S., Medrano, H., Or, E., Bavaresco, L., & Grando, S. (2010). Preface. In *Methodologies and*  
 313 *Results in Grapevine Research* (pp. 1–448). Springer Netherlands. <https://doi.org/10.1007/978-90->  
 314 481-9283-0  
 315

316 Diezma-Iglesias, B., Barreiro, P., Blanco, R., & García-Ramos, F. J. (2008). Comparison of robust  
 317 modeling techniques on NIR spectra used to estimate grape quality. *Acta Horticulturae*, 802, 367–  
 318 372. <https://doi.org/10.17660/ActaHortic.2008.802.48>  
 319

320 ElMasry, G., Wang, N., ElSayed, A., & Ngadi, M. (2007). Hyperspectral imaging for nondestructive  
 321 determination of some quality attributes for strawberry. *Journal of Food Engineering*, 81(1), 98–107.  
 322 <https://doi.org/10.1016/j.jfoodeng.2006.10.016>  
 323

324 FAO (Food and Agriculture Organization). (2009). Grapes Wine. In *FAO Agribusiness handbook* (p.  
 325 49). <http://www.fao.org/3/al176e/al176e.pdf>  
 326

327 Gallagher, N. B., Shaver, J. M., Martin, E. B., Morris, J., Wise, B. M., & Windig, W. (2004). Curve  
 328 resolution for multivariate images with applications to TOF-SIMS and Raman. *Chemometrics and*  
 329 *Intelligent Laboratory Systems*, 73(1 SPEC. ISS.), 105–117.  
 330 <https://doi.org/10.1016/j.chemolab.2004.04.003>  
 331

332 Guidetti, R., Beghi, R., & Bodria, L. (2010). Evaluation of grape quality parameters by a simple  
 333 VIS/NIR system. *Transactions of the ASABE*, 53(2), 477–484.

334

335 Guo, W., Li, W., Yang, B., Zhu, Z. Z., Liu, D., & Zhu, X. (2019). A novel noninvasive and cost-  
336 effective handheld detector on soluble solids content of fruits. *Journal of Food Engineering*,  
337 257(March), 1–9. <https://doi.org/10.1016/j.jfoodeng.2019.03.022>

338

339 Gutiérrez, S., Fernández-Novales, J., Diago, M. P., & Tardaguila, J. (2018a). On-the-go hyperspectral  
340 imaging under field conditions and machine learning for the classification of grapevine varieties.  
341 *Frontiers in Plant Science*, 9(July), 1–11. <https://doi.org/10.3389/fpls.2018.01102>

342

343 Gutiérrez, S., Tardaguila, J., Fernández-Novales, J., & Diago, M. P. (2018b). On-the-go hyperspectral  
344 imaging for the in-field estimation of grape berry soluble solids and anthocyanin concentration.  
345 *Australian Journal of Grape and Wine Research*, i, 127–133. <https://doi.org/10.1111/ajgw.12376>

346

347 Huang, Y., Lee, M. A., Thomson, S. J., & Reddy, K. N. (2016). Ground-based hyperspectral remote  
348 sensing for weed management in crop production. *International Journal of Agricultural and*  
349 *Biological Engineering*, 9(2), 98–109. <https://doi.org/10.3965/j.ijabe.20160902.2137>

350

351 Ishida, T., Kurihara, J., Viray, F. A., Namuco, S. B., Paringit, E. C., Perez, G. J., Takahashi, Y., &  
352 Marciano, J. J. (2018). A novel approach for vegetation classification using UAV-based hyperspectral  
353 imaging. *Computers and Electronics in Agriculture*, 144(December 2017), 80–85.  
354 <https://doi.org/10.1016/j.compag.2017.11.027>

355

356 Jay, S., Gorretta, N., Morel, J., Maupas, F., Bendoula, R., Rabatel, G., Dutartre, D., Comar, A., &  
357 Baret, F. (2017). Estimating leaf chlorophyll content in sugar beet canopies using millimeter- to  
358 centimeter-scale reflectance imagery. *Remote Sensing of Environment*, 198, 173–186.  
359 <https://doi.org/10.1016/j.rse.2017.06.008>

360

361 Liu, D., Zeng, X. A., & Sun, D. W. (2015). Recent Developments and Applications of Hyperspectral  
362 Imaging for Quality Evaluation of Agricultural Products: A Review. *Critical Reviews in Food Science*  
363 *and Nutrition*, 55(12), 1744–1757. <https://doi.org/10.1080/10408398.2013.777020>

364

365 Manley, M., Joubert, E., Myburgh, L., & Kidd, M. (2007). Prediction of soluble solids content and  
366 post-storage internal quality of Bulida apricots using near infrared spectroscopy. *Journal of Near*  
367 *Infrared Spectroscopy*, 15(3), 179–188. <https://doi.org/10.1255/jnirs.725>

368

369 Matese, A., & Di Gennaro, S. F. (2015). Technology in precision viticulture: A state of the art review.  
370 *International Journal of Wine Research*, 7(1), 69–81. <https://doi.org/10.2147/IJWR.S69405>

371

372 McGlone, V. A., & Kawano, S. (1998). Firmness, dry-matter and soluble-solids assessment of  
373 postharvest kiwifruit by NIR spectroscopy. *Postharvest Biology and Technology*, 13(2), 131–141.  
374 [https://doi.org/10.1016/S0925-5214\(98\)00007-6](https://doi.org/10.1016/S0925-5214(98)00007-6)

375

376 Munera, S., Besada, C., Blasco, J., Cubero, S., Salvador, A., Talens, P., & Aleixos, N. (2017).  
377 Astringency assessment of persimmon by hyperspectral imaging. *Postharvest Biology and*  
378 *Technology*, 125, 35–41. <https://doi.org/10.1016/j.postharvbio.2016.11.006>

379

380 Nicolaï, B. M., Beullens, K., Bobelyn, E., Peirs, A., Saeys, W., Theron, K. I., & Lammertyn, J. (2007).  
381 Nondestructive measurement of fruit and vegetable quality by means of NIR spectroscopy: A review.  
382 *Postharvest Biology and Technology*, 46(2), 99–118.  
383 <https://doi.org/10.1016/j.postharvbio.2007.06.024>

384



385 OIV (International Organisation of Vine and Wine). (2019). *2019 Statistical Report on World*  
386 *Vitiviniculture* (p. 23). <https://doi.org/64/19/6835> [pii]\n10.1158/0008-5472.CAN-04-1678  
387

388 Pellegrino, A., Lebon, E., Simonneau, T., & Wery, J. (2005). Towards a simple indicator of water  
389 stress in grapevine (*Vitis vinifera* L.) based on the differential sensitivities of vegetative growth  
390 components. *Australian Journal of Grape and Wine Research*, 11(3), 306–315.  
391 <https://doi.org/10.1111/j.1755-0238.2005.tb00030.x>  
392

393 Pu, H., Liu, D., Wang, L., & Sun, D. W. (2016). Soluble Solids Content and pH Prediction and  
394 Maturity Discrimination of Lychee Fruits Using Visible and Near Infrared Hyperspectral Imaging.  
395 *Food Analytical Methods*, 9(1), 235–244. <https://doi.org/10.1007/s12161-015-0186-7>  
396

397 Rinnan, Å., van den Berg, F., & Engelsen, S. B. (2009). Review of the most common pre-processing  
398 techniques for near-infrared spectra. *TrAC Trends in Analytical Chemistry*, 28(10), 1201–1222.  
399 <https://doi.org/10.1016/J.TRAC.2009.07.007>  
400

401 Teixeira Dos Santos, C. A., Lopo, M., Páscoa, R. N. M. J., & Lopes, J. A. (2013). A review on the  
402 applications of portable near-infrared spectrometers in the agro-food industry. *Applied Spectroscopy*,  
403 67(11), 1215–1233. <https://doi.org/10.1366/13-07228>  
404

405 Underwood, J., Wendel, A., Schofield, B., McMurray, L., & Kimber, R. (2017). Efficient in-field  
406 plant phenomics for row-crops with an autonomous ground vehicle. *Journal of Field Robotics*, 34(6),  
407 1061–1083. <https://doi.org/10.1002/rob.21728>  
408

409 Wendel, A., Underwood, J., & Walsh, K. (2018). Maturity estimation of mangoes using hyperspectral  
410 imaging from a ground based mobile platform. *Computers and Electronics in Agriculture*, 155(June),  
411 298–313. <https://doi.org/10.1016/j.compag.2018.10.021>  
412

413 Whetton, R. L., Waine, T. W., & Mouazen, A. M. (2018). Hyperspectral measurements of yellow  
414 rust and fusarium head blight in cereal crops: Part 2: On-line field measurement. *Biosystems*  
415 *Engineering*, 167, 144–158. <https://doi.org/10.1016/j.biosystemseng.2018.01.004>  
416

417 Zarco-Tejada, P. J., Guillén-Climent, M. L., Hernández-Clemente, R., Catalina, A., González, M. R.,  
418 & Martín, P. (2013). Estimating leaf carotenoid content in vineyards using high resolution  
419 hyperspectral imagery acquired from an unmanned aerial vehicle (UAV). *Agricultural and Forest*  
420 *Meteorology*, 171–172, 281–294. <https://doi.org/10.1016/j.agrformet.2012.12.013>

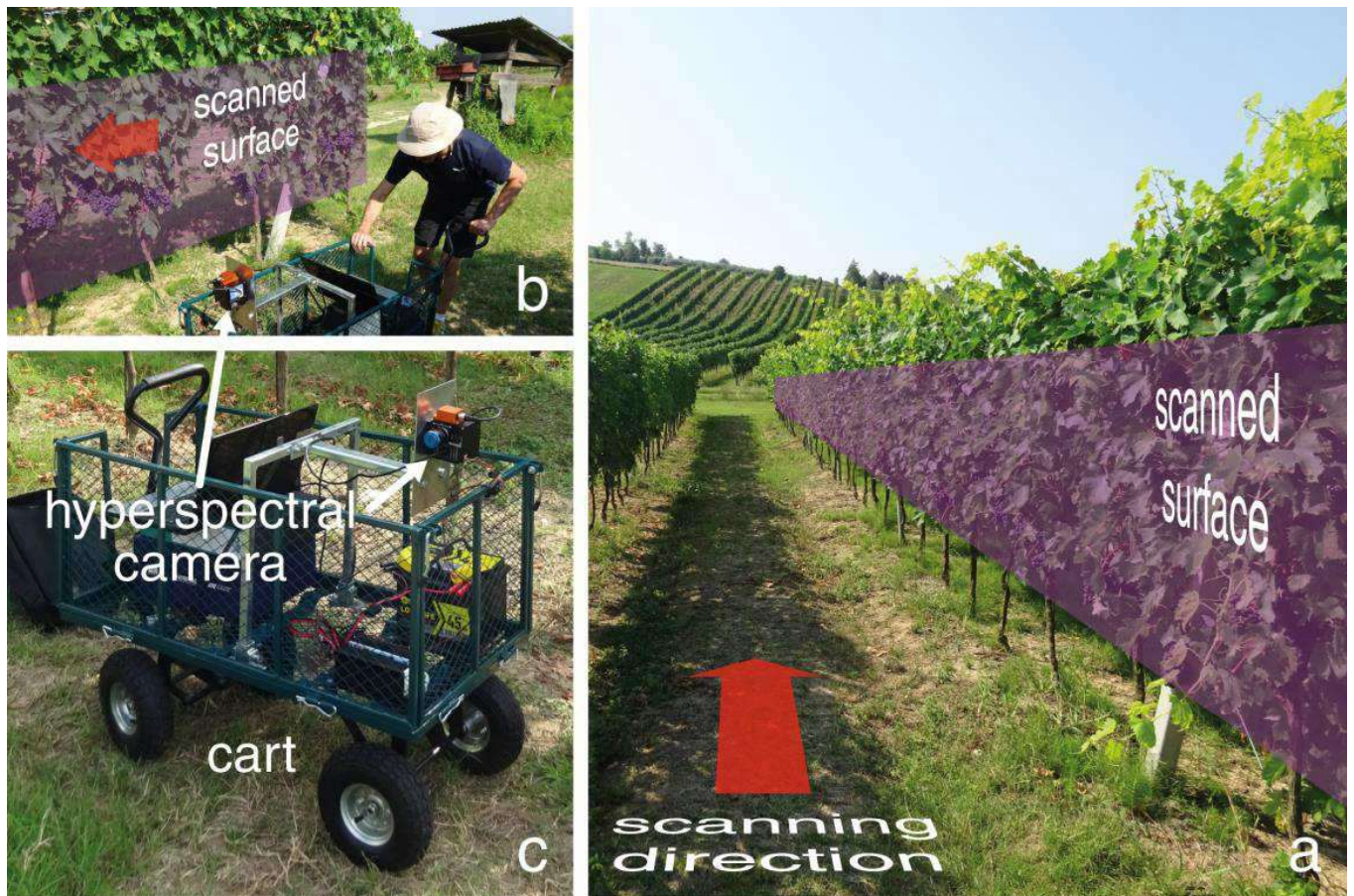


Fig.1

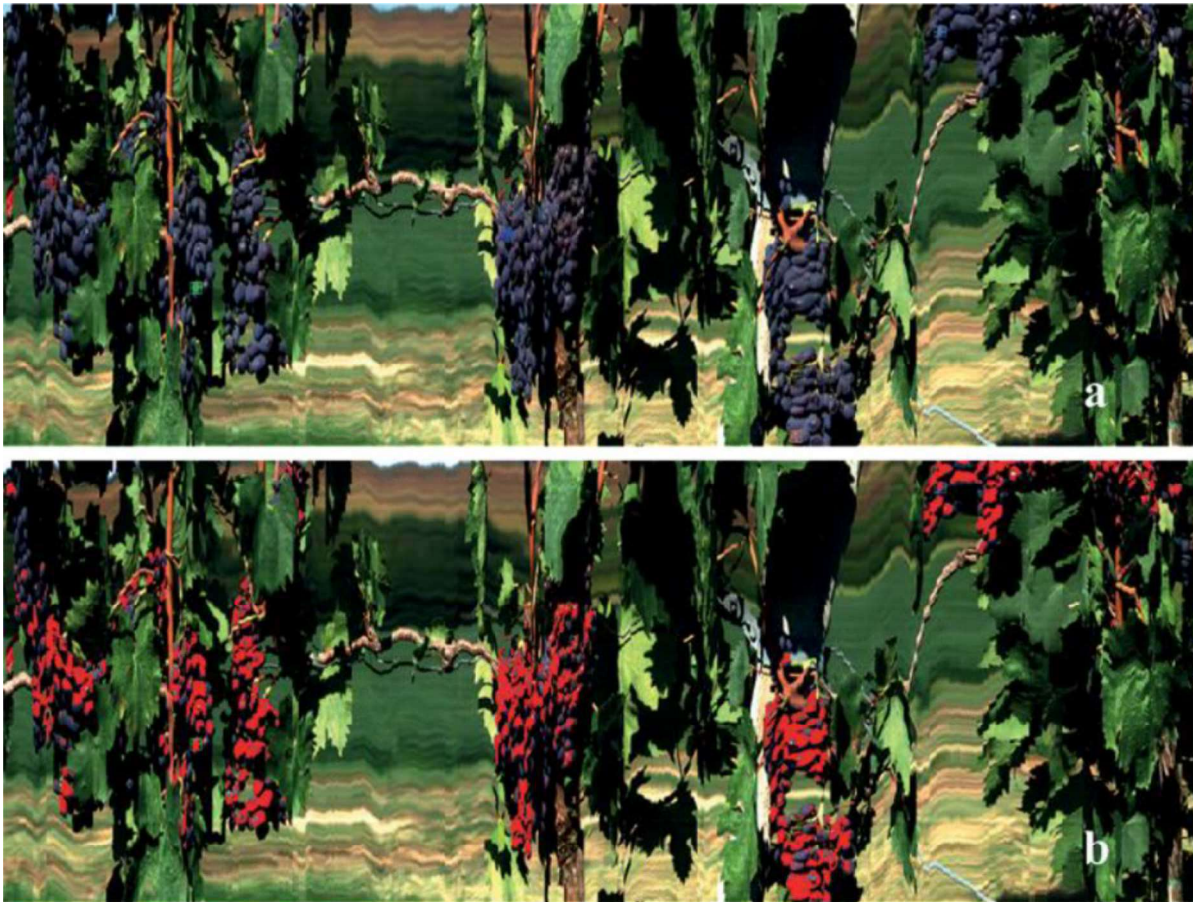


Fig. 2



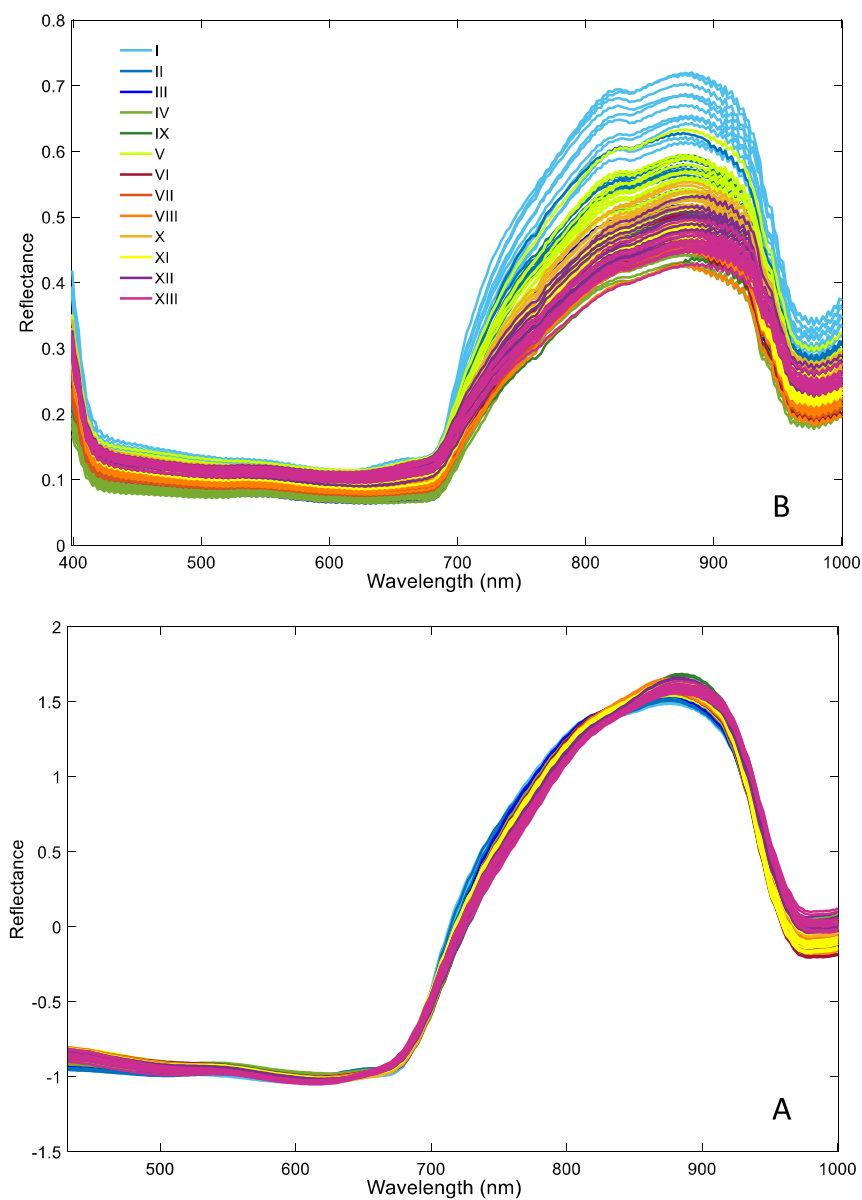


Fig. 3

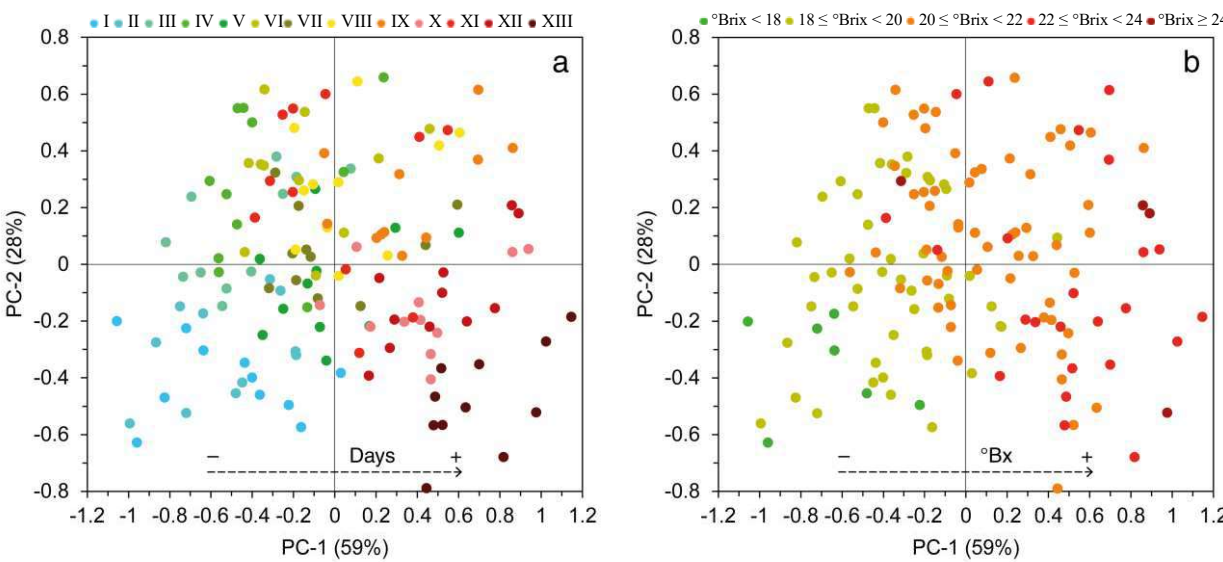


Fig. 4

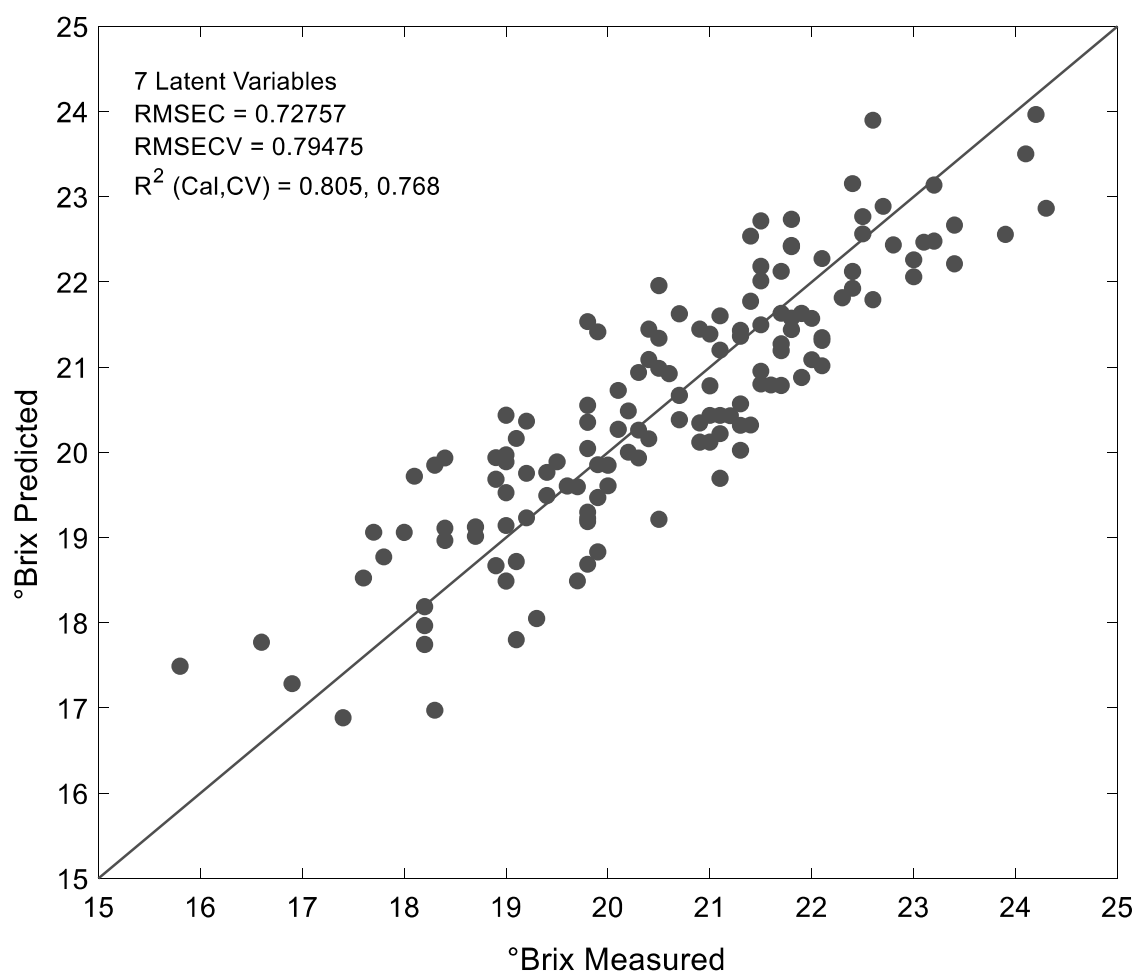


Fig. 5

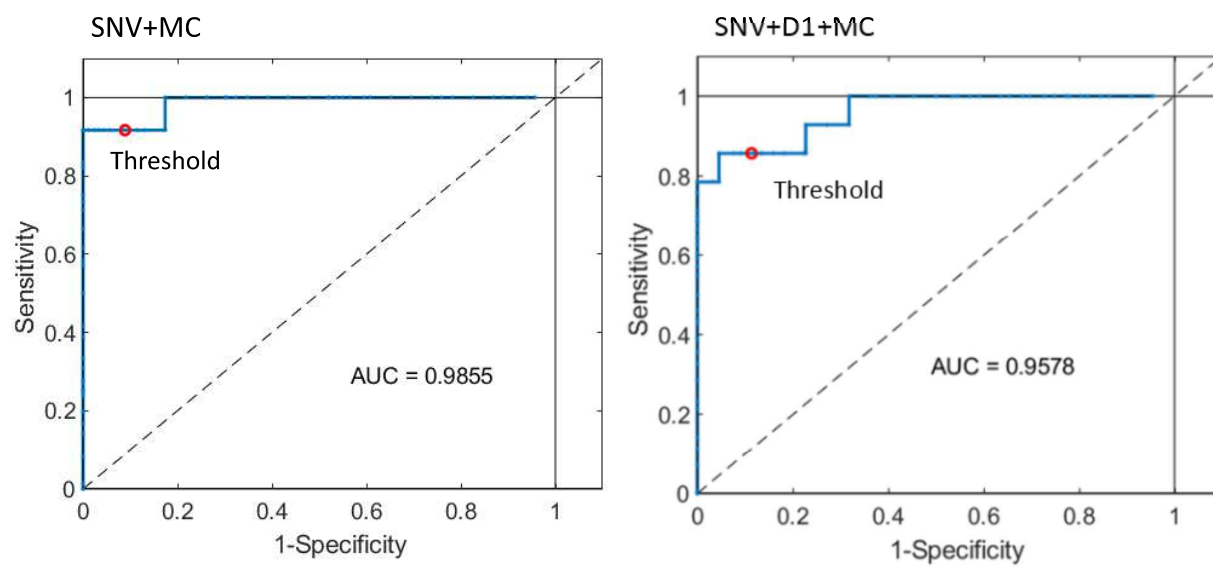


Fig. 6



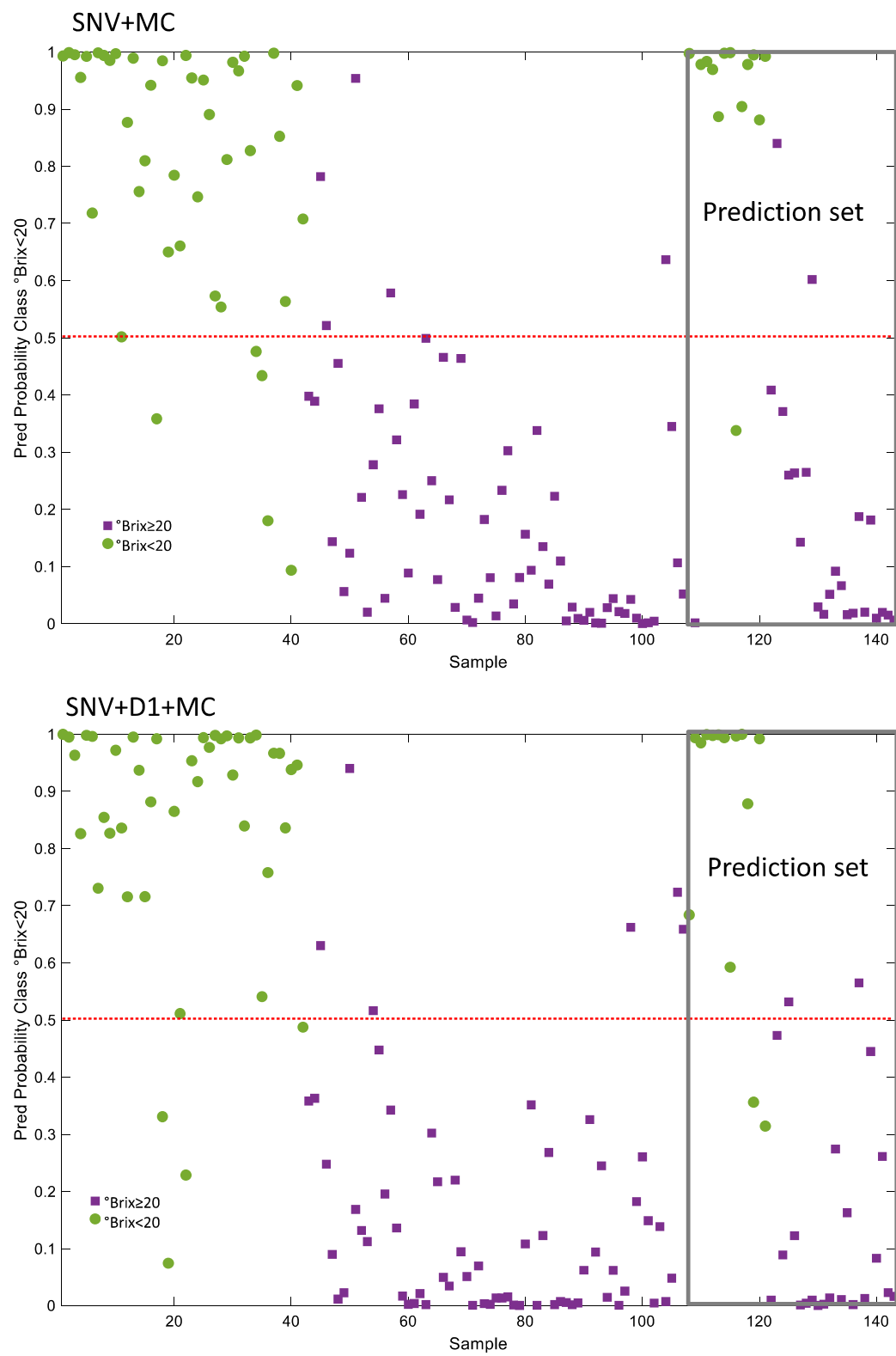


Fig. 7

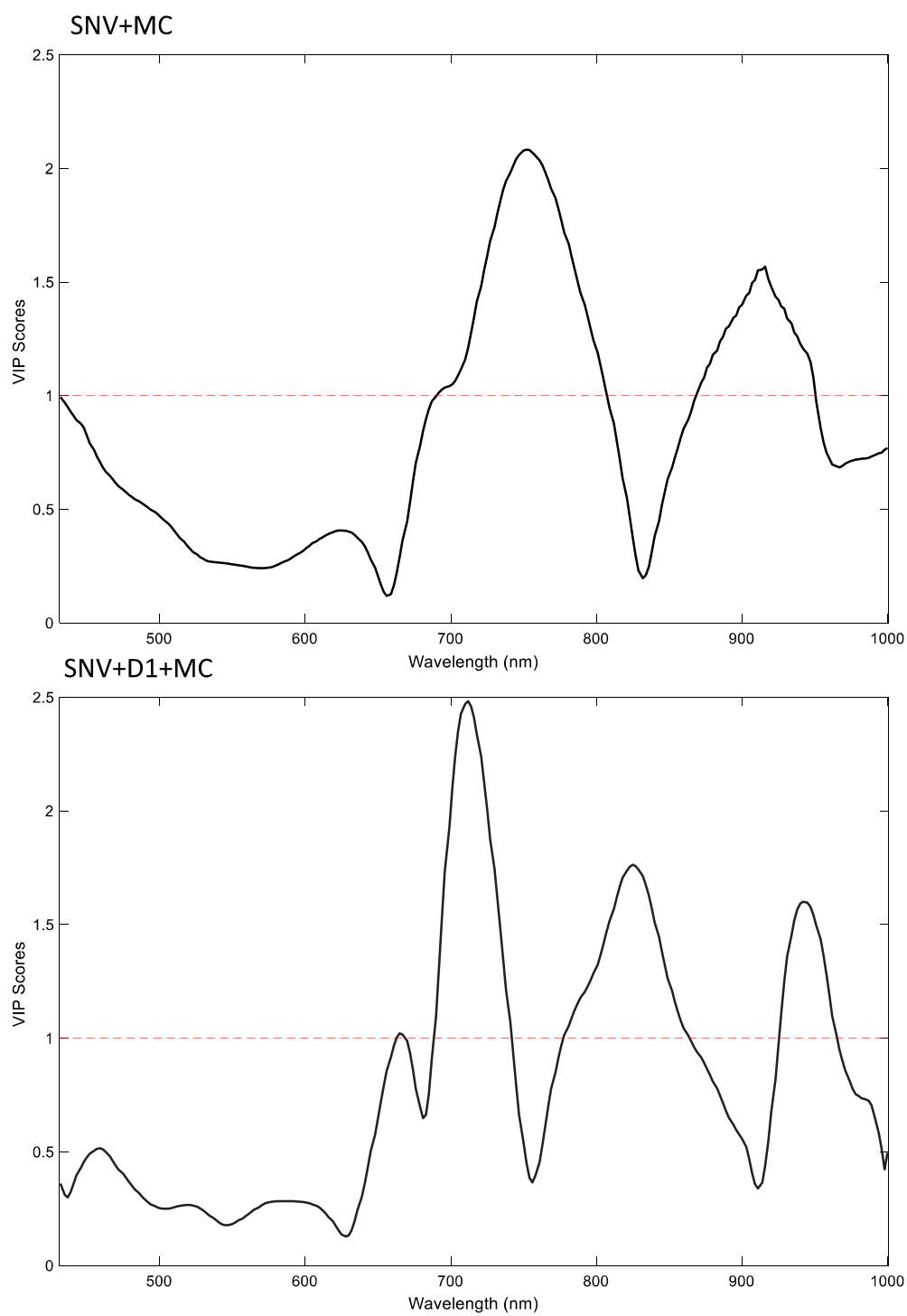


Fig. 8

1    **Figure captions**

2    **Fig. 1.** (a) Vineyard row, highlighted by the purple surface, scanned with the Vis/NIR hyperspectral  
3    camera; red arrow indicates the direction of scanning; (b) Garden cart mounted with hyperspectral  
4    camera. (c) In-field hyperspectral imaging to measure soluble solids content of wine grape berries  
5    during ripening.

6    **Fig. 2.** (a) RGB image from hyperspectral image of a scanned vineyard row section. (b)  
7    Representation of the ROI (in red) resulting from the classification obtained by the Manhattan  
8    function.

9    **Fig. 3.** Raw (A) and pre-treated by smoothing and SNV (B) spectra of all samples on different days  
10   of analysis (from I to XIII).

11   **Fig. 4.** Score plot obtained by the PCA according to: (a) days of analysis (from I to XIII); (b) soluble  
12   solids content (°Brix).

13   **Fig. 5.** Measured vs predicted values of solid soluble content (°Brix) obtained by PLS regression  
14   (cross validation).

15   **Fig. 6.** ROC curve of the PLS-DA models in prediction.

16   **Fig. 7.** Probability values of belonging to the class °Brix<20.

17   **Fig. 8.** VIP scores of the PLS-DA.

**Table 1.** Mean and standard deviation values of soluble solids content (°Brix) as a function of days of analysis.

Day of analisys	Mean (°Brix)	Standard deviation (°Brix)
I	17.8 <sup>a</sup>	1.05
II	19.0 <sup>a,b</sup>	0.81
III	19.2 <sup>b,c</sup>	0.75
IV	19.9 <sup>b,c,d</sup>	1.1
V	20.1 <sup>b,c,d</sup>	1.16
VI	20.2 <sup>b,c,d,e</sup>	0.95
VII	20.5 <sup>c,d,e,f</sup>	1.11
VIII	20.7 <sup>d,e,f</sup>	0.82
IX	21.5 <sup>e,f,g</sup>	0.76
X	21.6 <sup>e,f,g</sup>	0.89
XI	21.7 <sup>f,g</sup>	1.17
XII	22.7 <sup>g</sup>	0.94
XIII	22.7 <sup>g</sup>	0.88

*Note: means with the same letter are not significant different at p-level < 0.05.*

**Table 2.** PLS-DA results in terms of percentages of correctly classified samples (whole spectral range).

Spectra pretreatment	Class	Calibration (n=107)	Cross-validation (n=107, 10 segments)	Prediction (n=36)	LV
SNV+MC	°Brix<20	89%	89%	91%	4
	°Brix≥20	91%	91%	91%	
SNV+D1+ MC	°Brix<20	91%	89%	86%	4
	°Brix≥20	91%	91%	91%	

*Note: SNV=Standard Normal Variate; MC=Mean Cantered; D1=first derivative, LV=Latent Variable.*

**Table 3.** PLS-DA results in terms of percentages of correctly classified samples (reduced spectral range).

Spectra pretreatment	Class	Calibration (n=107)	Cross-validation (n=107, 10 segments)	Prediction (n=36)	LV
SNV+MC	°Brix<20	84%	83%	86%	4
	°Brix≥20	93%	92%	91%	
SNV+D1+ MC	°Brix<20	89%	89%	88%	3
	°Brix≥20	90%	87%	87%	

*Note: SNV=Standard Normal Variate; MC=Mean Cantered; D1=first derivative, LV=Latent Variable.*

<i>Nomenclature</i>	
AUC	area under the curve
CV	cross validation
D1	first derivative
HSI	hyperspectral imaging
MC	mean centring
NIR	near-infrared
PCA	principal component analysis
PLS	partial least squares
PLS-DA	partial least squares discriminant analysis
R	reflectance spectrum
RMSE	root mean square error
ROC	receiver operating characteristic
ROI	region of interest
SNV	standard normal variate
SSC	soluble solids content
SVM	support vector machines
VIP	variable importance in projection

**Declaration of interests**

☒ The authors declare that they have no known competing financial interests or personal relationships that could have appeared to influence the work reported in this paper.

☐The authors declare the following financial interests/personal relationships which may be considered as potential competing interests: